Automated Agricultural Crop Type Mapping Using Fusion of Transfer Learning and Tasmanian devil Optimization Algorithm on Remote Sensing Imagery

Daniel Arockiam[1,2,*], Azween Abdullah[3], Valliappan Raju[4]

[1]Postdoctoral Fellow, Perdana University, Kuala Lumpur 50490, Malaysia
[2]Amity University Madhya Pradesh, Gwalior 474005, India
[3]Faculty of Applied Science and Technology, Perdana University, Kuala Lumpur 50490, Malaysia
[4]Open & Dist. Learning Centre, Perdana University, Kuala Lumpur 50490, Malaysia

Emails: daniel.arockiam@perdanauniversity.edu.my; azween@perdanauniversity.edu.my; valliappan@perdanauniversity.edu.my

Abstract

At present, the application of remote sensing (RS) data achieved from satellite imagery or unmanned aerial vehicles (UAV) has become common for crop classification procedures, i.e. crop mapping, soil classification, or prediction of yield. The classification of food crop utilizing RS images (RSI) is one of the major applications of RS in farming. It contains the usage of aerial or satellite images for classifying and identifying dissimilar kinds of food crops developed in an exact region. This data is beneficial for estimation of yield, crop monitoring, and land management. Meeting the conditions for examining these data needs more refined techniques and artificial intelligence (AI) technologies, which deliver essential support. Recently, the usage of deep learning (DL) for crop type classification with RS images could help sustainable farming practices by providing appropriate and precise data on the kinds and features of crops. In this study, we offer an Automated Agricultural Crop Type Mapping Utilizing Fusion of Transfer Learning and Tasmanian Devil Optimization (AACTM-FTLTDO) algorithm on Remote Sensing Imagery. The primary goal of the AACTM-FTLTDO methodology is to accurately detect and classify crop types for more precise agricultural monitoring using remote sensing technologies. To accomplish that, the AACTM-FTLTDO model employs a fusion of transfer learning techniques involving three models such as SqueezeNet, CapsNet, and ShuffleNetV2 to capture diverse, multi-scale spatial and spectral features. For the crop type classification and detection process, the auto-encoder (AE) classifier can be employed. Eventually, the tasmanian devil optimization (TDO) technique was deployed to modify the hyperparameter of the AE technique for ensuring optimal model configurations and reducing computational complexity. A wide range of experimentation studies is made and the results are examined under numerous measures. The comparative study shows that the AACTM-FTLTDO technique performs better than existing approaches

Keywords: Crop Type Mapping; Remote Sensing Imagery; Tasmanian devil Optimization; Transfer Learning; Agricultural

1. Introduction

The monitoring of agricultural regions is of higher significance in the framework for worldwide challenges including increasing food demand, climate change, and population growth [1]. The world's possibly available cropland is inadequate and cropland growth is often connected with negative eco-logical effects like biodiversity loss and deforestation, especially for sensitive ecosystems [2]. Another approach to the rise in food production is the intensification of present croplands by optimized and enhanced management practices to close yield gaps. Efficiently and effectively monitoring agricultural production is important to tackling food insecurity problems

DOI: https://doi.org/10.54216/JCIM.150206
Received: April 29, 2024 Revised: June 25, 2024 Accepted: October 14, 2024

and supports farming management [3]. Fast improvement of Earth observation satellites offers a better opportunity to accomplish this condition worldwide. Particularly, uncharged and free access to satellite images is accelerating method enlargement for agricultural monitoring [4].

Remote Sensing Image (RSI) classification has been an active region of investigation for the last two years in regions including poverty mapping, agriculture, disaster management, and national security [5]. Crop classification helps as an important step for estimating the crop area coverage along with an early step for crop yield forecasting. Crop classification in RSI images is a significant application in land-use and agriculture monitoring. It recognizes and identifies several types of vegetation or crops in aerial or satellite images [6]. Remote sensing, mainly satellites provides an immense source of information for studying temporal and spatial variation in the environmental parameters [7]. Remote sensing has exposed better potential for identifying the crops grown on agricultural land. The resultant information is helpful for the estimation of crop production and utilization of land. It plays an significant part in yield assessment, crop health, and crop classification [8]. Since the initial stage of crop classification with digital RSI information, various methods that depend on unsupervised and supervised classification methods have been utilized to map the geographical distribution of crops with optical data and describe cropping practices [9]. In recent times, the more efficient and popular methods for multi-temporal and multi-sensor land cover classification are Deep Learning (DL) and Machine learning (ML) [10]. These methods are dominant for solving a wide variety of challenges emerging in Computer Vision (CV), processing RS imagery, and image processing.

In this study, we offer an Automated Agricultural Crop Type Mapping Utilizing Fusion of Transfer Learning and Tasmanian Devil Optimization (AACTM-FTLTDO) model on Remote Sensing Imagery. To accomplish that, the AACTM-FTLTDO model employs a fusion of TL techniques involving three models such as SqueezeNet, CapsNet, and ShuffleNetV2 to capture diverse, multi-scale spatial and spectral features. For the crop type classification and detection process, the auto-encoder (AE) classifier can be employed. Eventually, the tasmanian devil optimization (TDO) algorithm is deployed to fine-tune the hyperparameter of the AE technique for ensuring optimal model configurations and reducing computational complexity. A sequence of experimentation studies is made and the outcomes are examined under numerous aspects.

2. Related Works

In [11], a new DL-based method efficient for recognizing healthy and diseased leaves is projected through diverse crops, even though the method was not trained on them. For effective classification and to control the quality of the Inception method for the identification of diseases, a small Inception method structure is applied, which is suited for processing smaller areas without diminished performance. Alajmi et al. [12] introduce a dandelion optimizer with a Deep Transfer Learning-based Crop Type Detection and Classification (DODTL-CTDC) method on HSI. This method creates usage of the Xception method for feature extraction. Additionally, the hyper-parameter choice of the Xception method occurs utilizing the DO methodology. Furthermore, the CAE method is employed for the crop classification into different classes. Additionally, an Arithmetic Optimizer Algorithm (AOA) is applied for optimum hyper-parameter selection of the CAE method. Amri et al. [13] projected a new DL method particularly designed for classifying the different Saudi Arabia flora. To achieve these challenges, a new dataset was generated, called Saudi Arabia Flora Dataset, including samples from 10 different kinds of plants found in several areas of Saudi Arabia. The projected method, called MIV-PlantNet, controls the assets of 3 substantial architectures: Inception, VGG, and MobileNet.

Alahmari et al. [14] designed a Hybrid Multi-Strategy Aquila Optimizer with a DL-Driven CTC (HMAODL-CTC) method on HSI. This technique primarily performs image pre-processing for enhancing the excellence of the image. Additionally, the proposed HMAODL-CTC system improves the dilated CNN for the extraction of features. Designed for changing the hyper-parameter, the HMAO methodology is used. Finally, the proposed method utilizes an ELM method for classification of crop-type. Goyal et al. [15] proposed a DL-based custom CNN structure. A unique image database was shaped by obtaining RGB images. A custom-CNN method was built utilizing block features like dense layers, and fully connected layers, and comparing them with five advanced CNN architectures, that is Xception, EfficientNetB1, DenseNet121, InceptionV3, and ResNet50.

In [16], an automatic method was developed for precisely classifying and detecting diseases from a delivered photograph. The presented method accepts a CV-based method utilizing the approaches of DL, ML, and minimizing the reliance on traditional approaches to defend paddy crops from viruses. Subsequent image pre-processing and segmentation are applied for controlling the disease section. Incorporation of a SVM and CNNs techniques are applied to classify and recognize a particular variety of paddy plant diseases. In [17], an IoT-aid pest classification and identification approach is developed. Primarily, IoT sensors are employed to gather the essential images. Then, the input image is utilized to do recognition of the object completed by the Yolov3.

DOI: https://doi.org/10.54216/JCIM.150206
Received: April 29, 2024 Revised: June 25, 2024 Accepted: October 14, 2024

Moreover, the identified image is led into the method of CNN are transferred and eventually produced as an input to the classifying method of CNLSTM, few parameters are changed by Adaptive Honey Badger Algorithm (AHBA).

3. The Proposed Model

In this study, we offer an AACTM-FTLTDO algorithm on Remote Sensing Imagery. The primary goal of the AACTM-FTLTDO methodology is to accurately detect and classify crop types for more precise agricultural monitoring using remote sensing technologies. To accomplish that, the AACTM-FTLTDO model has distinct processes involved as a fusion of TL, AE-based crop type classification, and TDO-based parameter optimizer. Fig. 1 depicts the workflow of the AACTM-FTLTDO algorithm.

A. Fusion of Transfer Learning

Primarily, the AACTM-FTLTDO model employs a fusion of TL techniques involving three models such as SqueezeNet, CapsNet, and ShuffleNetV2 to capture diverse, multi-scale spatial and spectral features.

a) SqueezeNet Classifier

SqueezeNet is recognized as a particular type of Deep Neural Network (DNN), which is prepared for classifying images [18]. The initial determination of it is to maintain considerable levels of precision, however, they are smaller and more effective in comparison with another DNN.

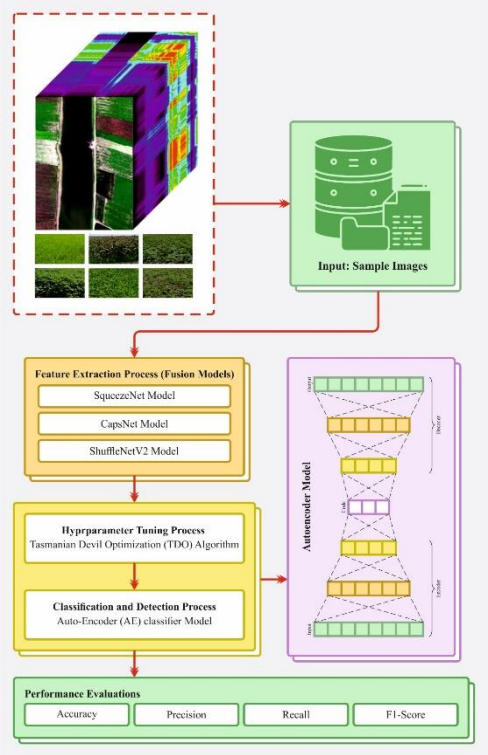

Figure 1. Workflow of AACTM-FTLTDO algorithm

There is a model applied in SqueezeNet to attain efficiency and smaller size named compression of the network. Based on this method, it substitutes the convolution layers, which are larger and costly with dense and effectual ones. It is attained by new applications incorporating 1x1 pooling and convolutional layers that may broadly reduce the variable's quantities within the network. Furthermore, it must be renowned that it includes Fire Modules. These modules, which are made from the squeeze and expansion layers are the constituent elements of the network.

A 1x1 size convolutions are utilized in the SqueezeNet layer to reduce the input channel quantities, while 3x3 and 1x1 size convolutions are combined in the expansion layer to improve the output channel quantities. Finally, the network might successfully collect local and global input images things. Possessing numerous classification stages presented results in a growth in the model's accuracy in comparison with dependency on a specific output classification. Deep supervision can improve the model precision that proposes myriad classification layers. The SqueezeNet model contains three different stages.

DOI: https://doi.org/10.54216/JCIM.150206
Received: April 29, 2024 Revised: June 25, 2024 Accepted: October 14, 2024

b) CapsNet Classifier

The CapsNet is a newly discovered innovative DL method that originated from CNN, using a novel computation element named capsule [19]. All capsules use a neuron group for learning a wide variety of features for a particular object existing in the image, comprising the present probabilities and instantiating parameters, such as orientation, deformation, location, size, and so on. It accepts an information vector output rather than a value of scale for feature examples and substitutes the pooling process in CNNs by dynamical routing of the feature spatial encoder. Hence, it is more informative for geographic objects and is better conducted for spatial data mining. Fig. 2 depicts the infrastructure of CapsNet.

In particular, every capsule contains a vector output and input. For a capsule j, its input s_i means the weighted summation of the predicted vector $\hat{u}$ from the output u_i of prior capsule i, that is Eq. (1):

$$s_j = \sum_i c_{ij}\, \hat{u}_{j|i} \hat{u}_{j|i} = W_{ij} u_j \tag{1}$$

Whereas W_{ij} denotes equivalent weight transformation W, and c_{ii} represents the coupling coefficient made by dynamical routing among others. Then, the vector output v_i is encouraged by a non-linear squashing function, as in Eq. (2):

$$v_j = \frac{\|s_j\|^2}{1 + \|s_j\|^2} \frac{s_j}{\|s_j\|^2} \tag{2}$$

Here its length indicates the present probabilities of targeted entities and its coordination designates different things of geographic entities. In this description, the disturbance generated by vector length is efficiently subdued, which is stronger than intra-class differences.

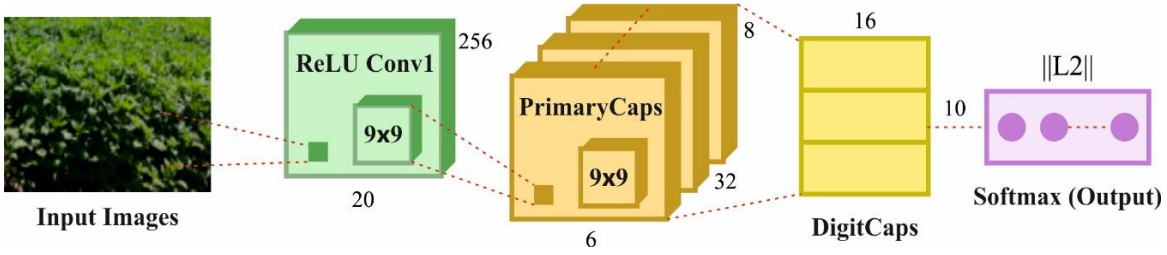

Figure 2. Structure of CapsNet

A classic CapsNet contains an auto encoder architecture, using an encoder consisting of various traditional layers, an initial capsule layer, the decoder, and an entity capsule layer comprising several fully connected (FC) layers. The convolutional layers have been used to remove the main features and make appropriate input for capsules. The initial capsule layer absorbs entity-related features in the way of vector expression. It is otherwise named the class capsule layer with a particular class. However, the FC layers in the decoding are used to rebuild an inputs depending on the vector output and encourage the encoding to acquire more informational features from an input data.

c) ShuffleNetV2 Classifier

The ShuffleNet-V2 system is a light-weight method that constructs over the ShuffleNetV1 structure [20]. The succeeding four main features can considerably influence the ShuffeNet-V2 networking speed. (i) If the output and input networks are equivalent, the method functions at its maximal speed using minimum memory access times. (ii) Extreme convolution processes can improve memory access times, leading to a slow speed of the model. (iii) The smaller amount the branches of the model, the more quickly the speed. (iv) Calculation point-wise processes can slow the model and the frequencies of these additions are minimalized.

It includes dual major modules: the basic unit and the down-sampling unit, respectively. During this basic unit, the features of an input image are separated uniformly into dual clusters below a channel-splitting process. The correct branch in sequence crosses the 1x1 convolution, a 1x1 convolution, and a 3x3 depth-wise convolution, however, the left branch stays natural. Then, the branches of the right and left are connected, and channel shuffling has been carried out to improve the information exchange among various groups. During this down-sampling, the image features may be directly arrived at two branches. This right branch experiences in sequence processing over a 1x1 convolution, 3x3 depthwise convolution by a stride of 2, and a 1x1 convolution.

DOI: https://doi.org/10.54216/JCIM.150206
Received: April 29, 2024 Revised: June 25, 2024 Accepted: October 14, 2024

B. Crop Type Classification using AE

For classification of crop type and detection process, the AE classifier can be employed. AE is a DL model applied to feature extraction and selection, depending on unsupervised learning, and utilizes backpropagation (BP) methods for learning the weighted parameters of the system [21]. The input and output vectors own similar dimensionalities since the network rebuilds its inputs after the training procedure.

AE condenses data into a low representation called code or bottleneck and attempts to rebuild the output from the bottleneck. An AE has 3 modules: Bottleneck, Encoder, and Decoder. The encoding aims to condense data into a lower size called bottleneck. The encoder is a Neural Networks (NNs) that has numerous layers; the bottleneck is finale layer. The below mentioned equation displays the process of every encoding layer:

$$X_{ei+1} = f\left(W_{e_i}^T X_{e_i} + b_{e_i}\right) \forall i = 0,1,2,\dots,N \quad (3)$$

For the $i\ th$ encoding layer:

X_{ei}: denotes input; W_{ei}: the weight; f_{ei}: the activation function; b_{ei}: the bias; X_{ei+1}: the result.

Generally, the Encoder is represented by the mathematic task below:

$$z = f(Wx + b) \quad (4)$$

Here, Z means latent code (size), f refers to the activation function, b and W are bias, and weight correspondingly.

The decoding rebuilds an input depending on latent space. The Decoder's input is an output of bottleneck layer (code). The decoding is stated by the succeeding Eq. (5):

$$X_{di+1} = f_{d_i}\left(W_{d_i}^T X_{d_i} + b_{d_i}\right) \forall i = 0,1,2,\cdots,N \quad (5)$$

For the $i\ th$ decoding layer:

X_{di}: the input; f_{di}: the activation function; b_{di}: the bias; W_{di}: the weight; X_{di+1}: the result.

Generally, the Decoder is signified by the calculation function under:

$$x' = f'(W'z + b') \quad (6)$$

The variance among the original data X^O and reconstructed data X^R is named Reconstruction Loss (RL). To reduce RL, BP method is applied for training the AE. To calculate the RL, we may utilize dual loss functions namely MSE and BCE. The mathematic expressions for these dual-loss functions are exposed in Eqs. (7) and (8):

$$MSE\left|(X^O, X^R) = \frac{1}{D}\Sigma_{j=1}^{D}\right|\left(X_j^o - X_j^R\right)^2 \quad (7)$$

$$BCE(X^0, X^R) = -\frac{1}{D}\sum_{j=1}^{D} X_j^0 \cdot \log X_j^R + \left(1 - X_j^0\right).log(1 - X_i^R) \quad (8)$$

C. TDO-based Parameter Optimizer

Eventually, the TDO technique is deployed to perfect the hyperparameter of AE technique to ensure optimal model configurations and reduce computational complexity. The process of optimization intends to discover optimum solutions to optimizer problems related to the Tasmanian demon food procedure [22]. This method includes exploring a complete search space and exploiting admittance to optimum solutions. The searching behavior of TD expressions the search index in the optimization procedure, while its search procedure was related to the local search exploitation.

Initialization

TDs help as search agents, making the foundation of recommended TDO, a metaheuristic model. A random population was initially recognized. Hence, every member of the population is technologically represented as a vector. Therefore, the matrix in Eq. (9) is employed for modelling the groups of TDO members.

$$P = \begin{bmatrix} P_1 \\ \vdots \\ P_i \\ \vdots \\ P_M \end{bmatrix} = \begin{bmatrix} p_{1,1} & \cdots p_{1,j} & \cdots p_{1,n} \\ \vdots & \ddots & \vdots \\ p_{i,1} & \cdots p_{i,j} & \cdots p_{i,n} \\ \vdots & \ddots & \vdots \\ p_{M,1} & \cdots p_{M,j} & \cdots p_{M,n} \end{bmatrix}_{M \times n} \quad (9)$$

DOI: https://doi.org/10.54216/JCIM.150206
Received: April 29, 2024 Revised: June 25, 2024 Accepted: October 14, 2024

Whereas P signifies the population of TDs, n implies the variable counts, M represents the searching TD counts, $p_{i,j}$ refers to its value as a candidate for the j^{th} variable, and P_i means i^{th} possible solution. A vector has been used for modelling the gained values for the objective function as presented in Eq. (10).

$$FiT = \begin{bmatrix} F_1 \\ \vdots \\ F_i \\ \vdots \\ F_M \end{bmatrix} = \begin{bmatrix} F(P_1) \\ \vdots \\ F(P_i) \\ \vdots \\ F(P_M) \end{bmatrix} \quad (10)$$

FiT symbolizes the fitness values, by F_i representing the value gained by every candidate solution. Calculating the values of objective function offers an understanding of the candidate solution qualities. The best members of the population are established by the candidate solution that generates the optimum value of the objective function. The fitness was calculated by the Eq. (11).

$$FiT = wt_1 \times C_c + wt_2 \times P + wt_3 \times K_L \quad (11)$$

Here P, K_L and C_c, denotes primality, length, and computational complexity. wt_1, wt_2, and wt_3 are weights that decide the importance of every condition.

Exploration

Local carrion is a favorite source of food for TDs instead of hunting. The occurrence of other hunters that pursue after the largest prey and leave remains makes a requirement for other food resources. In such cases, TDs select to consume carrion. Their model of pursuing carrion in their habitation is related to how methods discover solutions in problematic areas. The theories behind TD's feeding behavior, whereas they eat corpses, are signified by methods in Eqs. (12) - (14). Every TD considers the positions of another member of the population as possible carrion places inside the search space. The choice of a particular position is randomly pretended in Eq. (12), using the t^{th} member of the population being selected as the target carrion for the i^{th} TD.

$$D_i = P_l, i = 1,2, \dots, M, l \in \{1,2, \dots, M | l \neq i\} \quad (12)$$

A novel position is established for TD inside the searching area depending on the selected corpse. When the fitness value of the corpse is greater, then the animal travels to it; or else, it travels far away from it. This behavior is proven in Eq. (13). Finally, in this initial tactic, when a novel position for the TD is calculated, this location is determined only when it produces an enhanced fitness value; or else, the animal stays at its previous place. This process is specified in Eq. (14).

$$p_{i,j}^{T1,new} = \begin{cases} p_{i,j} + s \cdot \left(d_{i,j} - R \cdot p_{i,j}\right), F_{Di} < F_i; \\ p_{i,j} + s \cdot \left(p_{i,j} - c_{i,j}\right), otherwise \end{cases} \quad (13)$$

$$P_i = \begin{cases} P_i^{T1,new}, F_i^{T1,new} < F_i; \\ P_i, otherwise, \end{cases} \quad (14)$$

Now, $P_i^{T1,new}$ indicates the update position of the TD considers a novel tactic, R signifying a number generated at random that is both 1 and 2, F_{Di} represents the objective function value of the selected carriers, using s specifying arbitrary numbers inside the interval, $F_i^{T1,new}$ characterizes its recently computed value of the objective function, whereas the value $p_{i,j}^{T1,new}$ is established for the j^{th} variable.

(iii) Exploitation

Foraging and hunting are the next livings of the TD. There are dual phases for TD movement throughout the offensive. Next, in the second phase, it hunts the target to a halt and begins feeding after a while. Eqs. (15) - (17) are applied to simulate the choice of prey and attacking behavior.

During this next approach, the location of the prey is derived from the location of another member of the population. The kth member is arbitrarily chosen to be wild, and t refers to a spontaneously happening arbitrary integer among one and M opposite i. In Eq. (15) the prey selection procedure is pretended.

$$Q_i = P_l, i = 1,2, .., M, t \in \{1,2, , M | t \neq i\} \quad (15)$$

Here, Q_i i denotes chosen prey by the i^{th} TD.

If the location of the prey is established, the novel position of the TD is computed. When the projected fitness value of the selected prey is greater, it arrives at this novel location; or else, it travels away from the position. This

DOI: https://doi.org/10.54216/JCIM.150206
Received: April 29, 2024 Revised: June 25, 2024 Accepted: October 14, 2024

process is represented in Eq. (16). When the novel position for the Tasmanian demon improves the target function value, it substitutes the previous one as specified in Eq. (17).

$$p_{i,j}^{T2,new} = \begin{cases} p_{i,j} + s \cdot \left(q_{i,j} - R \cdot p_{i,j}\right), F_{Qi} < F_{i'}. \\ p_{i,j} + s \cdot \left(p_{i,j} - q_{i,j}\right), otherwise \end{cases} \quad (16)$$

$$P_i = \begin{cases} P_i^{T2,new}, F_i^{T2,new} < F_{i'}. \\ P_i, otherwise, \end{cases} \quad (17)$$

Here $P_i^{T2,new}$ characterizes the upgraded position of the i^{th} Tasmanian. F_{Qi} denotes the fitness of the selected prey, $F_i^{T2,new}$ means its recently computed value, and the value for j^{th} variable can be represented by $p_{i,j}^{T2,new}$.

A local search is related to a wildlife search nearly attack place. This TD's behavior proves how TDO is applied to unite best candidate solutions. TD pursuit preys on the position of the attack to imitate the search procedure. The TD's chase stage is modeled with Eq. (18) to (20). Presently, the location of the TD is defined as the center of the neighborhood where wildlife search occurs.

$$RAD = 0.01\left(1 - \frac{I}{I_{\max}}()\right) \quad (18)$$

$$p_{i,j}^{new} = p_{i,j} + (2s - 1) \cdot \ RAD \ \cdot p_{i,j} \quad (19)$$

$$P_i = \begin{cases} P_i^{new}, F_i^{new} < F_{i'}. \\ P_i, othherwise, \end{cases} \quad (20)$$

Now P_i^{new} signifies the upgraded position of the i^{th} TD in proximities to P_i, $p_{i,j}^{new}$ indicates its novel value for $j\ th$ variable, and F_i^{new} specifies its recently computed objective function value. $l_{\max}$ refers to maximal iteration counts permitted, 1 refers to the present iteration amount, and RAD signifies the radius of the neighborhood centered on a point that is attacked.

The TDO model originates a fitness function (FF) to reach improved performance of classification. It defines a positive number to suggest the enhanced efficiency of the candidate solution. Here, the minimization of the classifier rate of error is dignified as FF. Its calculation is expressed below.

$$fitness(x_i) = ClassifierErrorRate(x_i)$$
$$= \frac{no.of\ misclassified\ instances}{Total\ no.of\ instances} * 100 \quad (21)$$

4. Performance Validation

The performance evaluation of the AACTM-FTLTDO method is studied under the WHU-Hi database [23, 24]. This dataset is gathered and distributed by the research group of RSIDEA of Wuhan University, and it can aid as a benchmark database for exact classification of crop. The database includes of 1000 samples under nine class labels as described in Table 1.

Table 1: Details of Dataset

Class labels	Number of Instances
Corn	1000
Cotton	1000
Sesame	1000
Broad-leaf soybean	1000
Narrow-leaf soybean	1000
Rice	1000
Water	1000
Roads and houses	1000
Mixed weed	1000
Total number of Instances	1000

DOI: https://doi.org/10.54216/JCIM.150206
Received: April 29, 2024 Revised: June 25, 2024 Accepted: October 14, 2024

Fig. 3 presents the classifier results of the AACTM-FTLTDO algorithm. Figs. 3a-3b shows the confusion matrices with precise recognition and classification of every classes under 70%TRPH and 30%TSPH. Fig. 3c demonstrates the PR curve, representing superior performance across all class labels. Followed by, Fig. 3d exemplifies the ROC analysis, signifying capable results with better ROC values for different classes.

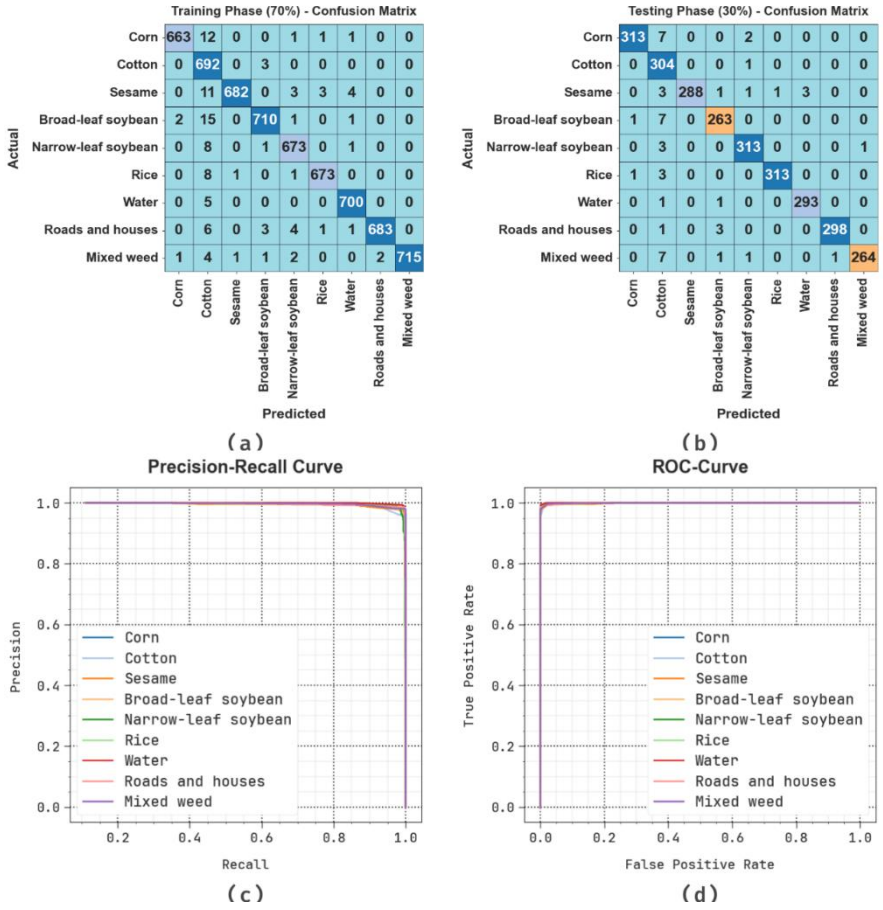

Figure 3. Classifier result of (a-b) 70% TRPH and 30% TSPH confusion matrix, (c) curve of PR, and (d) curve of ROC

Table 2 and Fig. 4 denote the crop type detection result of the AACTM-FTLTDO technique under 70%TRPH and 30%TSPH. The outcomes indicate that the AACTM-FTLTDO methodology properly recognized the samples. With 70%TRPH, the AACTM-FTLTDO system offers an average $accu_y$, $prec_n$, $reca_l$, and $F1_{score}$ of 99.62%, 98.35%, 98.27%, and 98.29%, respectively. Simultaneously, With 30%TSPH, the AACTM-FTLTDO approach offers average $accu_y$, $prec_n$, $reca_l$, and $F1_{score}$ of 99.58%, 98.22%, 98.08%, and 98.12%, correspondingly.

Table 2: Crop type detection of AACTM-FTLTDO model under 70%TRPH and 30%TSPH

Class Labels	$Accu_y$	$Prec_n$	$Reca_l$	$F1_{score}$
TRPH (70%)				
Corn	99.71	99.55	97.79	98.66
Cotton	98.86	90.93	99.57	95.05
Sesame	99.63	99.71	97.01	98.34
Broad-leaf soybean	99.57	98.89	97.39	98.13
Narrow-leaf soybean	99.65	98.25	98.54	98.39
Rice	99.76	99.26	98.54	98.90
Water	99.79	98.87	99.29	99.08
Roads and houses	99.73	99.71	97.85	98.77
Mixed weed	99.83	100.00	98.48	99.24

DOI: https://doi.org/10.54216/JCIM.150206
Received: April 29, 2024 Revised: June 25, 2024 Accepted: October 14, 2024

Average	99.62	98.35	98.27	98.29
TSPH (30%)				
Corn	99.59	99.37	97.20	98.27
Cotton	98.78	90.48	99.67	94.85
Sesame	99.67	100.00	96.97	98.46
Broad-leaf soybean	99.48	97.77	97.05	97.41
Narrow-leaf soybean	99.67	98.43	98.74	98.58
Rice	99.81	99.68	98.74	99.21
Water	99.81	98.99	99.32	99.15
Roads and houses	99.81	99.67	98.68	99.17
Mixed weed	99.59	99.62	96.35	97.96
Average	99.58	98.22	98.08	98.12

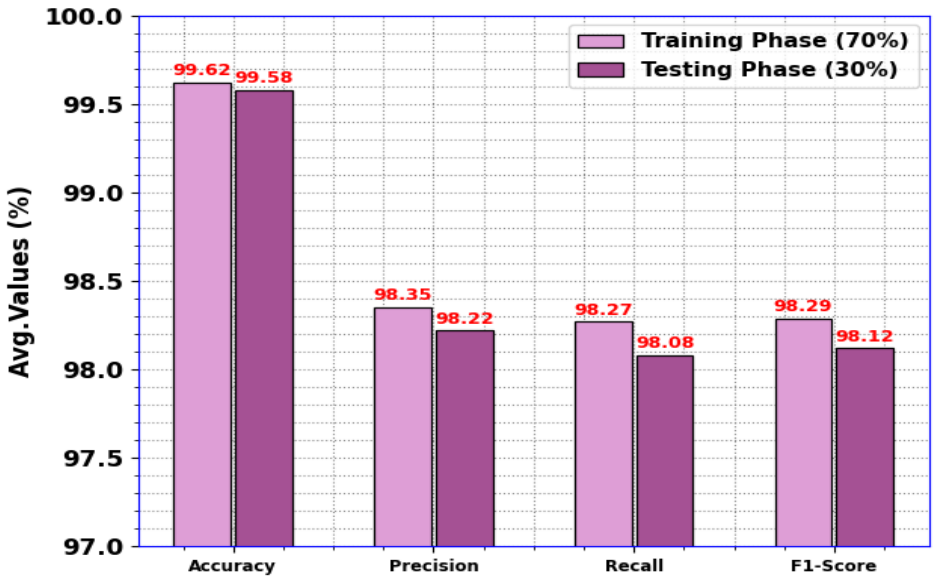

Figure 4. Average of AACTM-FTLTDO model under 70%TRPH and 30%TSPH

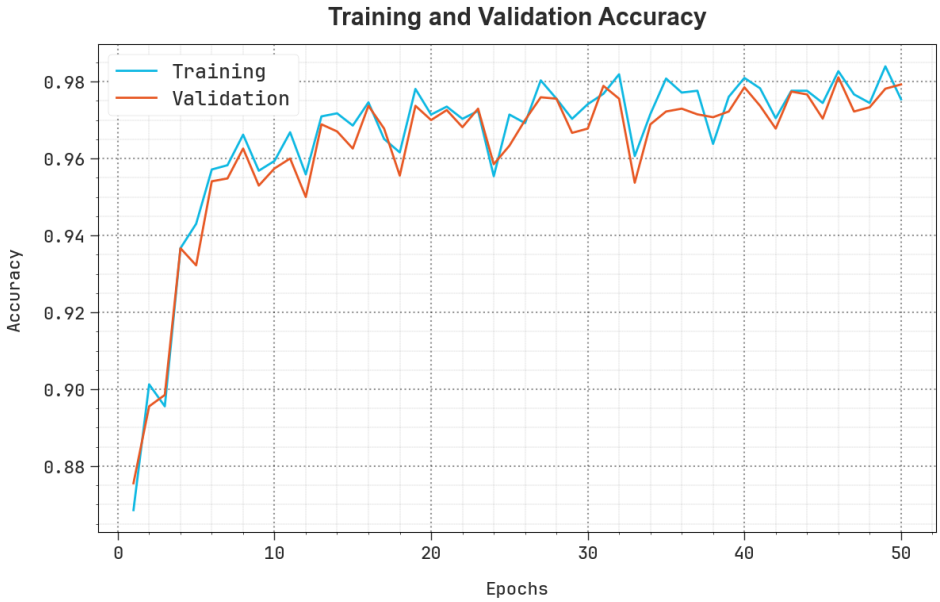

Figure 5. $Accu_y$ Curve of AACTM-FTLTDO model

DOI: https://doi.org/10.54216/JCIM.150206
Received: April 29, 2024 Revised: June 25, 2024 Accepted: October 14, 2024

In Fig. 5, the training (TRA) $accu_y$ and validation (VAL) $accu_y$ analysis of the AACTM-FTLTDO algorithm is exhibited. The $accu_y$ analysis are computed in the interval of 0-50 epochs. The figure highlighted that the TRA and VAL $accu_y$ analysis displays a rising trend which informed the capacity of AACTM-FTLTDO system with maximum performance over several iterations. Afterward, the TRA and VAL $accu_y$ remainders nearer over the epochs, which specifies inferior overfitting and demonstrates the higher performance of the AACTM-FTLTDO algorithm, guaranteeing reliable prediction on unseen models.

In Fig. 6, the TRA loss (TRALOS) and VAL loss (VALLOS) curves of the AACTM-FTLTDO method are shown. The values of loss are computed over the range of 0-50 epochs. It is denoted that the TRALOS and VALLOS analysis exemplifies a decreasing tendency, notifying the capacity of the AACTM-FTLTDO methodology to balance a trade-off between generalization and data fitting. The continual decrease in values of loss eventually ensures the maximal performance of the AACTM-FTLTDO algorithm and tunes the prediction results over time.

Figure 6. Loss graph of AACTM-FTLTDO system

Table 3 offers a comparative analysis of the AACTM-FTLTDO algorithm with existing methodologies in terms of $accu_y$ and processing time (PT) [12].

Fig. 7 represents the $accu_y$ analysis of AACTM-FTLTDO algorithm with existing methods. The simulation result stated that the AACTM-FTLTDO approach outperformed maximal performances. Based on $accu_y$, the AACTM-FTLTDO system has a maximum $accu_y$ of 99.62% where the SVM, FNEA-00, SVRFMC, CNN, CNN-CRF, SSODTL-CC, and DODTL-CTDC systems have lower $accu_y$ of 96.01%, 97.09%, 98.23%, 98.10%, 98.83%, 99.25%, and 99.49%, respectively.

Table 3: Comparative results of AACTM-FTLTDO model with existing techniques

Approach	$\boldsymbol{Accu_y}$ (%)	Processing Time (sec)
SVM Classifier	96.01	6.62
FNEA-00 Model	97.09	9.80
SVRFMC Method	98.23	7.59
CNN Methodology	98.10	9.89
CNN-CRF Model	98.83	11.31
SSODTL-CC	99.25	14.25
DODTL-CTDC	99.49	8.14
AACTM-FTLTDO	99.62	4.16

DOI: https://doi.org/10.54216/JCIM.150206
Received: April 29, 2024 Revised: June 25, 2024 Accepted: October 14, 2024

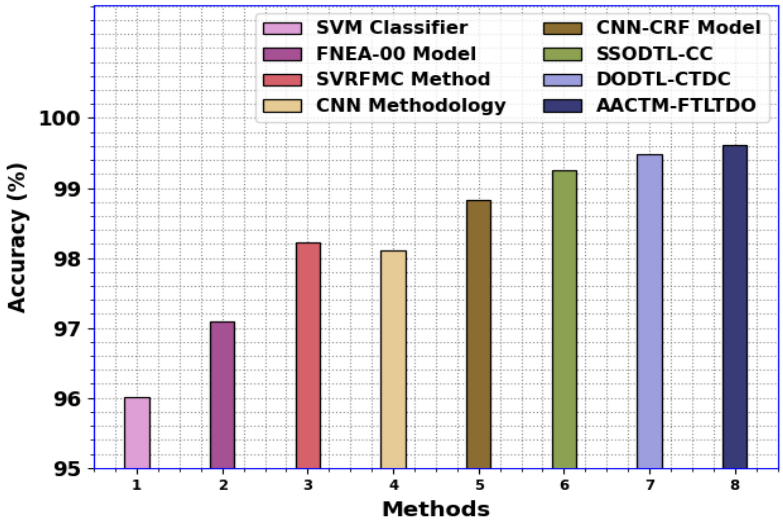

Figure 7. $Accu_y$ Analysis of AACTM-FTLTDO algorithm with existing model

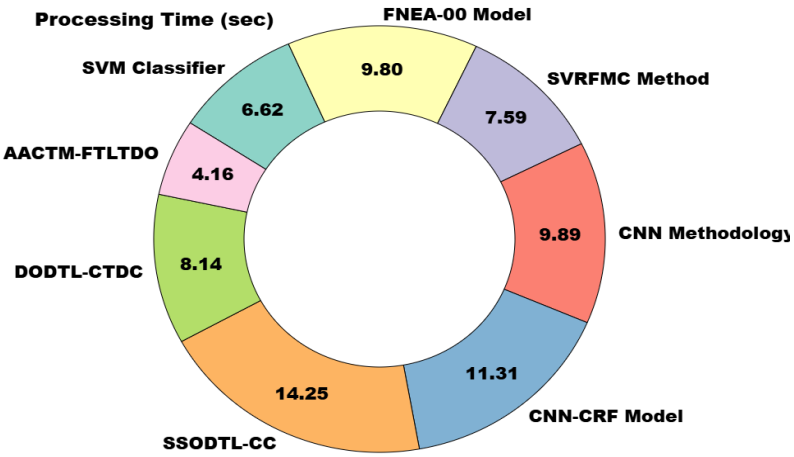

Figure 8. PT outcome of AACTM-FTLTDO methodology with existing approach

In Fig. 8, the comparative results of AACTM-FTLTDO approach is identified based on PT. The results recommend that the AACTM-FTLTDO model gets superior performance. Dependent on PT, the AACTM-FTLTDO approach offers inferior PT of 4.16s whereas the SVM, FNEA-00, SVRFMC, CNN, CNN-CRF, SSODTL-CC, and DODTL-CTDC models achieve greater PT values of 6.62s, 9.80s, 7.59s, 9.89s, 11.31s, 14.25s, and 8.14s, respectively.

5. Conclusion

In this study, we offer an AACTM-FTLTDO algorithm on Remote Sensing Imagery. The primary goal of the AACTM-FTLTDO methodology is to accurately detect and classify crop types for more precise agricultural monitoring using remote sensing technologies. To accomplish that, the AACTM-FTLTDO model employs a fusion of TL techniques involving three models such as SqueezeNet, CapsNet, and ShuffleNetV2 to capture diverse, multi-scale spatial and spectral features. For the crop type classification and detection process, the AE classifier can be employed. Eventually, the TDO technique is deployed to adjust the hyperparameter of the AE technique to ensure optimal model configurations and reduce computational complexity. A wide range of research examines is prepared and the results are reviewed under numerous features. The comparative study shows that the AACTM-FTLTDO technique performs better than existing approaches.

Funding: "This research received no external funding"

Conflicts of Interest: "The authors declare no conflict of interest."

DOI: https://doi.org/10.54216/JCIM.150206
Received: April 29, 2024 Revised: June 25, 2024 Accepted: October 14, 2024

References

[1] U. Patel, M. Pathan, P. Kathiria, and V. Patel, ‘‘Crop type classification with hyperspectral images using deep learning: A transfer learning approach,’’ Model. Earth Syst. Environ., vol. 9, no. 2, pp. 1977–1987, Jun. 2023.

[2] Li, H., Dou, X., Tao, C., Wu, Z., Chen, J., Peng, J., Deng, M. and Zhao, L., 2020. RSI-CB: A large-scale remote sensing image classification benchmark using crowdsourced data. Sensors, 20(6), p.1594.

[3] K. Bhosle and B. Ahirwadkar, ‘‘Deep learning convolutional neural network (CNN) for cotton, mulberry and sugarcane classification using hyperspectral remote sensing data,’’ J. Integr. Sci. Technol., vol. 9, no. 2, pp. 70–74, 2021.

[4] M. A. Duhayyim, H. Alsolai, S. B. H. Hassine, J. S. Alzahrani, A. S. Salama, A. Motwakel, I. Yaseen, and A. S. Zamani, ‘‘Automated deep learning driven crop classification on hyperspectral remote sensing images,’’ Comput., Mater. Continua, vol. 74, no. 2, pp. 3167–3181, 2023.

[5] P. Sadeghi-Tehran, N. Virlet, and M. J. Hawkesford, ‘‘A neural network method for classification of sunlit and shaded components of wheat canopies in the field using high-resolution hyperspectral imagery,’’ Remote Sens., vol. 13, no. 5, p. 898, Feb. 2021.

[6] Wei, W., Polap, D., Li, X., Woźniak, M. and Liu, J., 2018, November. Study on remote sensing image vegetation classification method based on decision tree classifier. In 2018 IEEE Symposium Series on Computational Intelligence (SSCI) (pp. 2292-2297). IEEE.

[7] K. Bhosle and V. Musande, ‘‘Evaluation of deep learning CNN model for land use land cover classification and crop identification using hyperspectral remote sensing images,’’ J. Indian Soc. Remote Sens., vol. 47, no. 11, pp. 1949–1958, Nov. 2019.

[8] Shi, J., Zhang, H., Jiang, Z. and Meng, G., 2019, October. Crop classification based on lightened convolutional neural networks in multispectral images. In Image and Signal Processing for Remote Sensing XXV (Vol. 11155, pp. 660-667). SPIE.

[9] Y. Zhang, D. Wang, and Q. Zhou, ‘‘Advances in crop fine classification based on hyperspectral remote sensing,’’ in Proc. 8th Int. Conf. AgroGeoinformatics (Agro-Geoinformatics), Jul. 2019, pp. 1–6.

[10] Elngar, A.A., Arafa, M., Fathy, A., Moustafa, B., Mahmoud, O., Shaban, M. and Fawzy, N., 2021. Image classification based on CNN: a survey. Journal of Cybersecurity and Information Management, 6(1), pp.18-50.

[11] Bouacida, I., Farou, B., Djakhdjakha, L., Seridi, H. and Kurulay, M., 2024. Innovative deep learning approach for cross-crop plant disease detection: A generalized method for identifying unhealthy leaves. Information Processing in Agriculture.

[12] Alajmi, M., Mengash, H.A., Eltahir, M.M., Assiri, M., Ibrahim, S.S. and Salama, A.S., 2023. Exploiting hyperspectral imaging and optimal deep learning for crop type detection and classification. IEEE Access, 11, pp.124985-124995.

[13] Amri, E., Gulzar, Y., Yeafi, A., Jendoubi, S., Dhawi, F. and Mir, M.S., 2024. Advancing automatic plant classification system in Saudi Arabia: introducing a novel dataset and ensemble deep learning approach. Modeling Earth Systems and Environment, 10(2), pp.2693-2709.

[14] Alahmari, S., Yonbawi, S., Racharla, S., Lydia, E.L., Ishak, M.K., Alkahtani, H.K., Aljarbouh, A. and Mostafa, S.M., 2023. Hybrid Multi-Strategy Aquila Optimization with Deep Learning Driven Crop Type Classification on Hyperspectral Images. Comput. Syst. Sci. Eng., 47(1), pp.375-391.

[15] Goyal, P., Sharda, R., Saini, M. and Siag, M., 2024. A deep learning approach for early detection of drought stress in maize using proximal scale digital images. Neural Computing and Applications, 36(4), pp.1899-1913.

[16] Haridasan, A., Thomas, J. and Raj, E.D., 2023. Deep learning system for paddy plant disease detection and classification. Environmental monitoring and assessment, 195(1), p.120.

[17] Kathole, A.B., Vhatkar, K.N. and Patil, S.D., 2024. IoT-enabled pest identification and classification with new meta-heuristic-based deep learning framework. Cybernetics and Systems, 55(2), pp.380-408.

[18] Duan, R., Lin, D. and Fathi, G., 2024. PEMFC model identification using a squeezenet developed by modified transient search optimization algorithm. Heliyon, 10(6).

[19] Zhai, H. and Zhao, J., 2024. Two-Stream spectral-spatial convolutional capsule network for Hyperspectral image classification. International Journal of Applied Earth Observation and Geoinformation, 127, p.103614

[20] Yu, Y.N., Xiong, C.L., Yan, J.C., Mo, Y.B., Dou, S.Q., Wu, Z.H. and Yang, R.F., 2024. Citrus Pest Identification Model Based on Improved ShuffleNet. Applied Sciences, 14(11), p.4437.

[21] Boukhris, A., Jilali, A. and Asri, H., 2024. Deep Learning and Machine Learning Based Method for Crop Disease Detection and Identification Using Autoencoder and Neural Network. Revue d'Intelligence Artificielle, 38(2)

DOI: https://doi.org/10.54216/JCIM.150206
Received: April 29, 2024 Revised: June 25, 2024 Accepted: October 14, 2024

[22] Almotairi, S., Addula, S.R., Alharbi, O., Alzaid, Z., Hausawi, Y.M. and Almutairi, J., Personal Data Protection Model in IOMT-Blockchain on Secured Bit-Count Transmutation Data Encryption Approach.

[23] http://rsidea.whu.edu.cn/resource_WHUHi_sharing.htm

[24] Y. Zhong, X. Hu, C. Luo, X. Wang, J. Zhao, and L. Zhang, "WHU-Hi: UAV-borne hyperspectral with high spatial resolution (H2) benchmark datasets and classifier for precise crop identification based on deep convolutional neural network with CRF", Remote Sens. Environ., vol. 250, pp. 112012, 2020.

DOI: https://doi.org/10.54216/JCIM.150206
Received: April 29, 2024 Revised: June 25, 2024 Accepted: October 14, 2024